

Meson loops in the $f_0(980)$ and $a_0(980)$ radiative decays into ρ , ω

H. Nagahiro¹, L. Roca² and E. Oset³

¹ Research Center for Nuclear Physics (RCNP), Ibaraki, Osaka 567-0047, Japan

² Departamento de Física. Universidad de Murcia. E-30071 Murcia. Spain
and the Yukawa Institute for Theoretical Physics, Kyoto University, Kyoto 606-8502, Japan

³ Departamento de Física Teórica and IFIC, Centro Mixto Universidad de Valencia-CSIC,
Institutos de Investigación de Paterna, Aptdo. 22085, 46071 Valencia, Spain

October 27, 2018

Abstract. We calculate the radiative decay widths of the $a_0(980)$ and $f_0(980)$ scalar mesons into $\rho\gamma$ and $\omega\gamma$ considering the dynamically generated nature of these scalar resonances within the realm of the Chiral Unitary Approach. The main ingredient in the evaluation of the radiative width of the scalar mesons are the loops coming from the decay into their constituent pseudoscalar-pseudoscalar components and the subsequent radiation of the photon. The dominant diagrams with only pseudoscalar mesons in the loops are found to be convergent while the divergence of those with a vector meson in the loop are written in terms of the two meson loop function easily regularizable. We provide results for all the possible charge channels and obtain results, with uncertainties, which differ significantly from quark loops models and some version of vector meson dominance.

PACS. 14.40.Cs – 13.25.Jx – 13.40.Hq

1 Introduction

The radiative decay of resonances has been advocated as a privileged tool to study the nature of resonances [1,2]. A good example of the interest in these reactions is offered by the large amount of works devoted to the study of the radiative decay of the $D_{s0}^*(2317)$ charmed scalar meson [3]. The uncharmed scalar mesons are the object of much debate regarding its nature as a possible $q\bar{q}$ state, a meson-meson molecule, a dynamically generated object from the interaction of pseudoscalar meson pairs in coupled channels or a hybrid of those structures [4,5,6,7]. The idea that the light scalar mesons $\sigma(600)$, $f_0(980)$, $a_0(980)$, $\kappa(800)$ are bound states or resonances formed from the interaction of pseudoscalar mesons has been gaining support, particularly because the underlying interaction is well known from the chiral Lagrangians [8], and then using any reasonable nonperturbative tools, like the Bethe Salpeter equation [7,9,10,11], the N/D method [12] or the Inverse Amplitude Method [13,14] the scalar states appear automatically. The support for this picture is also strengthened by the success reproducing different reactions where these resonances are produced without the need to introduce any free parameters. Examples of this are the description of the $\phi \rightarrow \pi^0\pi^0\gamma$ reaction with its strong $f_0(980)$ peak, or the $\phi \rightarrow \pi^0\eta\gamma$ reaction with its prominent $a_0(980)$ peak [15,10,16], the $\gamma\gamma \rightarrow \pi\pi$ and $\gamma\gamma \rightarrow K\bar{K}$ reactions [17,18] and, adjusting some normalization parameters, the description of the $J/\Psi \rightarrow N\bar{N}\pi\pi$

[19] and the $J/\Psi \rightarrow \omega\pi\pi$, $J/\Psi \rightarrow \phi\pi\pi$, with clear signals for the $\sigma(600)$ in the first reaction and of $f_0(980)$ in the second one [20,21]. The apparent narrowness of the $\sigma(600)$ in the $J/\Psi \rightarrow \omega\pi\pi$ reaction is nicely interpreted in [21] since the strength of σ production is proportional to the ratio t/V , with t the scalar isoscalar $\pi\pi$ amplitude and V the potential in the same channel (the Adler term). The narrowness is due to the strong energy dependence of the Adler term, which grows faster than the scattering t -matrix. Further considerations concerning the scalar meson sector are done in [22].

The success of the chiral unitary approach in describing the scalar sector and in particular the $f_0(980)$ and $a_0(980)$ resonances, can be further tested with new observables like those we suggest in the present work. Given the fact that the $\phi \rightarrow \pi^0\pi^0\gamma$ and $\phi \rightarrow \pi^0\eta\gamma$ reactions are well understood within this picture, one can look at the crossed channel reactions of the former ones in places where the energy conservation allows it. This is the case of the $f_0(980)$ and $a_0(980)$ resonances decaying into $V\gamma$ where V is now a vector meson which replaces the ϕ to make the reaction energetically possible. Such vector mesons can only be the ρ and the ω . The sensitivity of this observable to details of different models is huge and has been discussed in several works, assuming vector meson dominance and direct coupling of the scalar to VV [23], or quark loop contribution [1] or meson-meson loop contribution, $K\bar{K}$ [1], and $K\bar{K}$ and $\pi\pi$ [24]. The work presented here will follow the ideas of the chiral unitary

approach used to describe the $\phi \rightarrow \pi^0\pi^0\gamma$ decay, evaluating loops of $K\bar{K}$ and $\pi\pi$, as in the former works, but also those containing one vector meson, which proved to be relevant in the study of the radiative decay of vector mesons to two pseudoscalar mesons and one photon [25, 16]. An experimental proposal to measure the f_0, a_0 , to $V\gamma$ decays has been approved at COSY/WASA [26].

2 Formalism

By using the techniques of the unitary extensions of chiral perturbation theory (chiral unitary approach or Unitarized ChPT) the low lying scalar resonances ($\sigma, \kappa, f_0(980)$ and $a_0(980)$), among many other mesonic and baryonic resonances, are generated dynamically. With the only input of the low-lying chiral Lagrangians, the implementation of unitarity in coupled channels and the exploitation of the analytic properties of the scattering amplitudes, the approach generates poles in unphysical Riemann sheets of the unitarized meson-meson scattering amplitudes which can be associated to those resonances. Hence they qualify as quasibound states of their constituent meson-meson components. Furthermore, by evaluating the residue of the meson-meson scattering amplitudes at the pole positions, this picture provides the value, including the phase, of the couplings of these resonances to their constituent building blocks. Indeed, close to the pole position the Laurent expansion of the scattering amplitude in a particular isospin and partial wave can be approximated by its dominant term

$$t_{ij} \simeq \frac{g_i g_j}{s - s_p}, \tag{1}$$

where i and j refer to a given meson-meson estate and $s_p \simeq (M - i\Gamma/2)^2$ is the pole position, with M and Γ the mass and width of the associated resonance. Hence, g_i in Eq. (1) can be identified as the coupling of the dynamically generated resonance (with the quantum numbers of the amplitude t) to the $i - th$ channel. In particular, using the Bethe-Salpeter unitarization procedure, we obtain the couplings of the a_0 and f_0 to their constituent pseudoscalar-pseudoscalar (PP) components shown in table 1. The difference with the results of ref. [27] will be considered as an uncertainty in the error analysis in the present work.

| i | g_i | $ g_i $ | $ g_i $ from ref. [27] |
|---------------|-----------------|---------|------------------------|
| $f_0\pi\pi$ | $469 - i1247$ | 1332 | 1100 |
| $f_0K\bar{K}$ | $-3369 - i1606$ | 3732 | 3680 |
| $a_0K\bar{K}$ | $-4732 - i943$ | 4825 | 5500 |
| $a_0\pi\eta$ | $3166 - i712$ | 3245 | 3900 |

Table 1. Couplings of the $f_0(980)$ and $a_0(980)$ to their different pseudoscalar-pseudoscalar constituent channels. All the units are in MeV.

Once we have these couplings, the philosophy we follow in order to obtain the radiative decay widths is al-

most straightforward: one has to consider the transition from the scalar mesons to the possible PP at one loop and then attach the photon to the possible allowed places, considering that a vector meson in the final state needs to be produced. For reasons that will be clear later on, the diagrams that we need to evaluate are only those shown in fig. 1.

The channels we will consider are $f_0 \rightarrow \rho^0\gamma, f_0 \rightarrow \omega\gamma, a_0^0 \rightarrow \rho^0\gamma, a_0^0 \rightarrow \omega\gamma$ and $a_0^+ \rightarrow \rho^+\gamma$. In fig. 1, S represents the decaying scalar mesons; P_1, P_2 , pseudoscalar mesons and V_1, V_2 , vector mesons. In the Appendix, tables 5-7, we show the different allowed $P_1P_2V_1V_2$ particles of the diagrams in fig. 1 together with the corresponding coefficients for each channel to be explained latter on. In fig. 1, P, q, k and Q represent the momentum of the different lines that will be used in the evaluation of the loop function.

At this point we take advantage of the implications of gauge invariance to simplify the calculations. We follow a similar procedure as done in refs. [28,15] in the evaluation of the radiative ϕ decay and in refs. [29,30] for the radiative axial-vector meson decays.

The general expression of the amplitude for the radiative decay of a scalar meson into a vector meson and a photon ($S \rightarrow V\gamma$) can be written as

$$T = \epsilon_{V\mu}\epsilon_\nu T^{\mu\nu} \tag{2}$$

with

$$T^{\mu\nu} = a g^{\mu\nu} + b Q^\mu Q^\nu + c Q^\mu k^\nu + d k^\mu Q^\nu + e k^\mu k^\nu \tag{3}$$

where Q is the final vector meson momentum and k the photon momentum, which are the only independent available momenta. In Eq. (2), ϵ_ν and ϵ are the vector meson and photon polarization vectors respectively. On the other hand, due to the Lorenz condition, $\epsilon_{V\mu}Q^\mu = 0, \epsilon_\nu k^\nu = 0$, all the terms in Eq. (3) vanish except for the a and d terms. Furthermore, gauge invariance implies that $T^{\mu\nu}k_\nu = 0$, from where one gets

$$a = -d Q \cdot k. \tag{4}$$

Therefore the amplitude gets the general form

$$T = -d(Q \cdot k g^{\mu\nu} - k^\mu Q^\nu)\epsilon_{V\mu}\epsilon_\nu. \tag{5}$$

Hence, we only need to evaluate those diagrams contributing to the d -term, that is, those having a final structure $k^\mu Q^\nu$. The advantage to evaluate only the d coefficient is that only the loop diagrams of fig. 1 contribute since other diagrams, like those involving photon couplings to the vertices which are necessary to fulfill gauge invariance, do not give contribution to the d coefficient [28,15, 29]. Another advantage is that, from dimensional reasons (performing explicitly the Feynman integrals), we will see that the d coefficients are finite for the type-a diagrams of fig. 1, while the logarithmic divergence from the type-b diagram can be easily identified and regularized by expressing it in terms of the two meson loop function of the PP scattering problem.

With the previous discussion in mind, let us explain the explicit steps in the calculation of the radiative decay

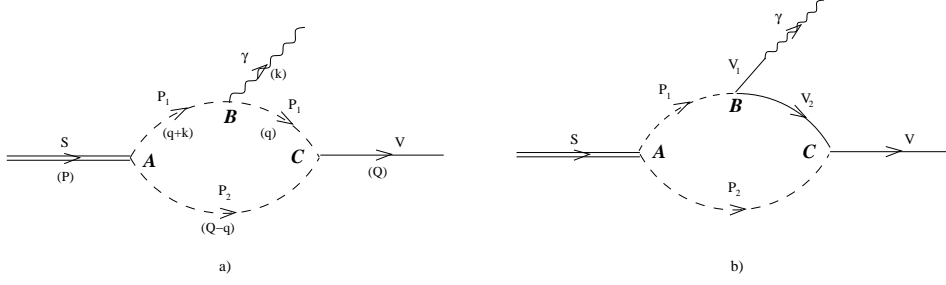


Fig. 1. Feynman diagrams contributing to the scalar radiative decays

width. We will consider first the evaluation of the type-a diagram of fig. 1. The Lagrangians needed in the evaluation of the type-a diagram in fig. 1 are, for the vector-pseudoscalar-pseudoscalar (VPP) vertex:

$$\mathcal{L}_{VPP} = -i \frac{g}{\sqrt{2}} \langle V^\mu [\partial_\mu P, P] \rangle \quad (6)$$

where $g = -M_V G_V / f^2$, with M_V the vector meson mass and G_V a coupling constant defined in [31] and for which we use the numerical value $G_V = 55 \pm 5$ MeV from ref. [16]. In Eq. (6), V and P are the $SU(3)$ matrices containing the octets of vector and pseudoscalar mesons respectively, see *e.g.* ref. [31], and $\langle \rangle$ means that one has to perform the trace of the $SU(3)$ resulting matrix. In Eq. (6), f is the pion decay constant ($f = 93$ MeV), however one can assign an uncertainty to the f constant since it could range from f_π to f_η . For the calculations we will actually use, as central value, $f = 1.08 \times 93$ MeV and we will also consider uncertainties in our calculations by taking a range of f between f_π and $1.15 f_\eta$.

The $PP\gamma$ vertex can be readily obtained from the lowest order ChPT Lagrangian [8]

$$\mathcal{L} = \frac{f^2}{4} \langle D_\mu U^\dagger D^\mu U \rangle \quad (7)$$

from where the $PP\gamma$ amplitude follows:

$$-it_{PP\gamma} = -iQ_i e \epsilon_\mu (p_1 + p_2)^\mu \quad (8)$$

with $p_1(p_2)$ the momentum of the ingoing(outgoing) pseudoscalar meson, Q_i is the sign of the charge of the pseudoscalar meson and e is taken positive.

Therefore, the amplitude for the type-a diagrams takes the form:

$$\begin{aligned} -it_a &= -iA g_{SP_1P_2} \int \frac{d^4q}{(2\pi)^4} \frac{i}{(q+k)^2 - m_1^2 + i\epsilon} \\ &\times \frac{i}{q^2 - m_1^2 + i\epsilon} \frac{i}{(Q-q)^2 - m_2^2 + i\epsilon} \\ &\times (-i) e Q_1 \epsilon_\nu (q + q + k)^\nu \\ &\times (-i) C \frac{M_V G_V}{\sqrt{2} f^2} \epsilon_{V\mu} (q - Q + q)^\mu, \end{aligned} \quad (9)$$

where A are coefficients given in table 5 needed to relate the SP_1P_2 coupling in charge basis with those in isospin

basis and with the unitary normalization of refs. [7], $g_{SP_1P_2}$. In Eq. (9) Q_1 is the sign of the charge of the P_1 pseudoscalar meson, $m_1(m_2)$ is the mass of the $P_1(P_2)$ pseudoscalar meson, M_V the mass of the final vector meson and C are coefficients coming from the Lagrangian of Eq. (6) after performing the trace of the matrix and which depend on the particular P_1, P_2 and V particles (specifically, C is the coefficient of $\langle V^\mu [\partial_\mu P, P] \rangle$ of Eq. (6) defined as $C(P_1 \partial P_2 - P_2 \partial P_1)$). The different A, C , coefficients are given in the Appendix, table 5.

By using the Lorenz condition, $\epsilon_{V\mu} Q^\mu = 0$ and $\epsilon_\nu k^\nu = 0$, the amplitude reads

$$\begin{aligned} t_a &= iA g_{SP_1P_2} e Q_1 C \frac{M_V G_V}{\sqrt{2} f^2} 4 \epsilon_{V\mu} \epsilon_\nu \\ &\times \int \frac{d^4q}{(2\pi)^4} q^\mu q^\nu \frac{1}{(q+k)^2 - m_1^2 + i\epsilon} \frac{1}{q^2 - m_1^2 + i\epsilon} \\ &\times \frac{1}{(Q-q)^2 - m_2^2 + i\epsilon}, \end{aligned} \quad (10)$$

This loop integral can be easily done by using the Feynman parametrization. We use the identity

$$\frac{1}{abc} = 2 \int_0^1 dx \int_0^x dy \frac{1}{[a + (b-a)x + (c-b)y]^3}. \quad (11)$$

We set

$$\begin{aligned} a &= (Q-q)^2 - m_2^2, \\ b &= q^2 - m_1^2, \\ c &= (q+k)^2 - m_1^2 \end{aligned} \quad (12)$$

and perform the change of variable

$$q = q' + (1-x)Q - yk. \quad (13)$$

Now we have to recall the above discussion in order to keep in mind that we only need the d coefficient (see Eqs. (3) and (5)). That means that we only need the terms producing a final structure of the type $k^\mu Q^\nu$, which reduce considerably the number of terms and, more important, the resulting expression contributing to the d -term is just finite. Thus the apparent superficial logarithmically divergent type-a loop (see Eq. (9) becomes pure convergent and, hence, with no need for regularization, it is univocally defined (no regularization parameters, scale, etc).

For the type-a loop, the final, simple and finite, expression for the d -coefficient of Eqs. (3) and (5), from where the amplitude can be obtained by using Eq. (5), is

$$d_a = AC Q_1 g_{SP_1 P_2} \sqrt{2} e \frac{M_V G_V}{f^2} \frac{1}{8\pi^2} \int_0^1 dx \int_0^x dy \frac{(1-x)y}{s+i\epsilon} \quad (14)$$

where $s = Q^2 x(1-x) + 2Q \cdot k(1-x)y + (m_2^2 - m_1^2)x - m_2^2$.

In the final step of the derivation of Eq. (14), since the remaining $d^4 q'$ integration is finite, we have used that [32]

$$\int d^4 q' \frac{1}{(q'^2 + s + i\epsilon)^3} = i \frac{\pi^2}{2} \frac{1}{s + i\epsilon}. \quad (15)$$

So far, what we have done corresponds to the meson loop calculation of [1, 24] with a significant difference, which is the coupling of the scalar resonance to the two pseudoscalar mesons. In [1] it is taken from [33] obtained using the Weinberg compositness condition [34], and as quoted in [1, 24] the estimation of the coupling should be viewed as qualitative [sic] [1]. Furthermore, only $K\bar{K}$ loops are contained in [1]. In [24], $\pi\pi$ loops are also considered and the couplings of the scalar to the pseudoscalar mesons are taken from the effective resonance Lagrangians of [31]. One should note in this respect that, while the vectors can be considered as genuine new fields, additional to the pseudoscalar ones, the scalar fields cannot be considered at the same level since they come from the same pseudoscalar-pseudoscalar Lagrangians after a proper unitarization [7, 12, 9, 10, 11]. This means that the use of a proper unitary theory involving the pseudoscalar-pseudoscalar meson chiral Lagrangians and the scalar resonance Lagrangians of [31] leads to double counting. On the other hand, assuming that these scalar resonance Lagrangians are only a means of providing at tree level the couplings of the scalar to pseudoscalar mesons, there are also problems since the a_0 and f_0 properties cannot be simultaneously fitted with the structure of the resonance Lagrangians of [31]. In our case, as explained above, the couplings are taken from the residues at the poles of the unitarized meson-meson interaction amplitudes, which reproduce very accurately the experimental data in a range of energies from threshold to 1.2 GeV and are consistent with a large variety of physical processes.

The other novelty of our approach is the evaluation of the type-b loops. The idea to include these loops stems from the relevance of intermediate vector mesons in the radiative decay of ρ, ω , into meson-meson-photon [25].

For the evaluation of the type-b loops, we first need the $V\gamma$ vertex given by

$$t_{V\gamma} = -F_V e \lambda_V M_V \epsilon_V \cdot \epsilon_\gamma, \quad (16)$$

where λ_V is 1, 1/3, $-\sqrt{2}/3$ for $V = \rho, \omega, \phi$ respectively, F_V is the coupling constant in the normalization of [31] for which we use the value $F_V = 156 \pm 5$ MeV [16].

For the VVP vertex we use the Lagrangian [35, 36]:

$$\mathcal{L}_{VVP} = \frac{G'}{\sqrt{2}} \epsilon^{\mu\nu\alpha\beta} \langle \partial_\mu V_\nu \partial_\alpha V_\beta P \rangle, \quad (17)$$

where $G' = 3g'^2/(4\pi^2 f)$ with $g' = -G_V M_\rho / (\sqrt{2} f^2)$. Since in the type-b loops we have two vertices of the type VVP , the amplitude is proportional to G'^2 or g'^4 . Hence, the contributions to the decay width of the type-b loops go like g'^8 . This means that small differences in the value of g' are strongly magnified in the evaluation of the radiative decays widths from the type-b mechanisms. Therefore a good numerical value for the VVP couplings is called for. Hence, in order to fine tune the numerical value of the VVP coupling constant we proceed as follows. From

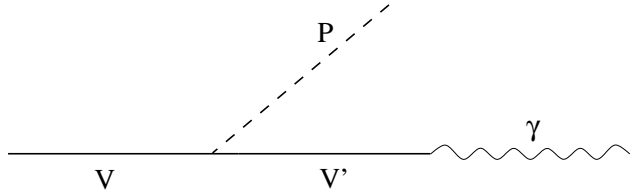


Fig. 2. $V \rightarrow P\gamma$ decay diagram

Eqs. (16) and (17), the decay width of the decay of a vector meson into a pseudoscalar meson and a photon, $V \rightarrow P\gamma$, (see fig. 2), takes the form:

$$\Gamma_{V \rightarrow P\gamma} = \frac{e^2}{24\pi} \left(\frac{B_i G' F_V \lambda_{V'}}{M_{V'}} \right)^2 |\mathbf{k}|^3. \quad (18)$$

where B_i are numerical coefficients depending on the different VVP channels that will be explicitly defined later on, and $|\mathbf{k}|$ is the center of mass momentum of the photon or the pseudoscalar meson. In table 2 we show the theoretical branching ratios together with the experimental ones [37]. The agreement with the experimental data is fair but

| i | BR_i^{th} | BR_i^{exp} |
|--|-----------------------|---------------------------------|
| $\rho^\pm \pi^\pm \gamma$ | 3.6×10^{-4} | $(4.5 \pm 0.5) \times 10^{-4}$ |
| $\rho^0 \pi^0 \gamma$ | 3.6×10^{-4} | $(6.0 \pm 0.8) \times 10^{-4}$ |
| $\rho^0 \eta \gamma$ | 3.1×10^{-4} | $(2.7 \pm 0.4) \times 10^{-4}$ |
| $\omega \pi^0 \gamma$ | 6.06% | $8.91 \pm 0.24\%$ |
| $\omega \eta \gamma$ | 6.5×10^{-4} | $(4.8 \pm 0.4) \times 10^{-4}$ |
| $K^{*+} \rightarrow K^+ \gamma$ $K^{*-} \rightarrow K^- \gamma$ | 9.3×10^{-4} | $(9.9 \pm 0.9) \times 10^{-4}$ |
| $K^{*0} \rightarrow K^0 \gamma$ $\bar{K}^{*0} \rightarrow \bar{K}^0 \gamma$ | 19.1×10^{-4} | $(23.1 \pm 2.0) \times 10^{-4}$ |

Table 2. Theoretical and experimental branching ratios for different vector meson decay processes.

the results can be improved by incorporating $SU(3)$ breaking mechanisms. For that purpose, we will normalize here the G' coupling by multiplying it by $N_i \equiv \sqrt{BR_i^{exp}/BR_i^{th}}$, dependent on the particular channel, such that the theoretical branching ratios agree with experiment. For the evaluation of the second column of table 2 and in the rest of the paper we fix $G' = 0.098$ MeV $^{-1}$. The experimental errors in table 2 will be considered later on when evaluating the uncertainties of our final results for the scalar radiative decays.

The amplitude for the type-b diagram of fig. 1 reads

$$\begin{aligned}
-it_b &= -iA g_{SP_1P_2} \int \frac{d^4q}{(2\pi)^4} iB \frac{N_B G'}{\sqrt{2}} F_V M_{V_1} e\lambda_{V_1} \frac{1}{M_{V_1}^2} \\
&\times \epsilon^{\mu\nu\alpha\beta} k_\mu \epsilon_\nu q_\alpha iC \frac{N_C G'}{\sqrt{2}} \epsilon^{\mu'\nu'\alpha'\beta'} Q_{\mu'} q_{\alpha'} \epsilon_{V\nu'} \\
&\times \frac{i}{(q+k)^2 - m_1^2 + i\epsilon} \frac{i}{(Q-q)^2 - m_2^2 + i\epsilon} \\
&\times \frac{i}{q^2 - M_2^2 + i\epsilon} \left(-g_{\beta\beta'} + \frac{q_\beta q_{\beta'}}{M_2^2} \right) \quad (19)
\end{aligned}$$

where $M_1(M_2)$ is the mass of the $V_1(V_2)$ vector meson. In Eq. (19), A has the same meaning as in the type-a loop case and B is the coefficient of the $P_1 V_1 V_2$ vertex obtained after performing the $SU(3)$ trace in $\langle VVP \rangle$ (see Eq. (17)) defined as $B P_1 V_1 V_2$. Analogously, C is the coefficient coming from the $P_2 V_2 V$ vertex defined as $C P_2 V V_2$ from the resulting expression after taking the trace in $\langle VVP \rangle$. The N_B and N_C couplings are the normalization factors for the B and C VVP vertices just that the $V \rightarrow P\gamma$ decays agree with experiment, as explained above. In the evaluation of the type-b loops we use for each VVP vertex a value of N_i obtained from the average of the different charge channels of table 2 containing the same vectors.

The loop integral in Eq. (19) is apparently quadratically divergent, the highest degree of divergence coming from the last $q_\beta q_{\beta'}$ term from the propagator of the vector meson in the loop. However, this last term gives zero contribution since $q_\alpha q_{\alpha'} q_\beta q_{\beta'}$ is a totally symmetric tensor and vanishes when contracting it with the antisymmetric Levi-Civita tensor.

Thus, the remaining logarithmically divergent amplitude reads:

$$\begin{aligned}
t_b &= -iA g_{SP_1P_2} B \frac{N_B G'}{\sqrt{2}} F_V e\lambda_{V_1} \frac{1}{M_{V_1}} C \frac{N_C G'}{\sqrt{2}} \\
&\times \int \frac{d^4q}{(2\pi)^4} \epsilon^{\mu\nu\alpha\beta} \epsilon^{\mu'\nu'\alpha'\beta'} k_\mu q_\alpha Q_{\mu'} q_{\alpha'} \epsilon_\nu \epsilon_{V\nu'} \\
&\times \frac{1}{(q+k)^2 - m_1^2 + i\epsilon} \frac{1}{(Q-q)^2 - m_2^2 + i\epsilon} \\
&\times \frac{1}{q^2 - M_2^2 + i\epsilon} \quad (20)
\end{aligned}$$

Even though the previous expression is logarithmically divergent, the divergence can be isolated and expressed in terms of the two-meson loop function that appears in the unitarization procedure of the meson-meson scattering amplitudes. The reasoning is as follows: by using that

$$\epsilon^{\mu\nu\alpha\beta} \epsilon^{\mu'\nu'\alpha'\beta'} = - \begin{vmatrix} g^{\mu\mu'} & g^{\mu\nu'} & g^{\mu\alpha'} \\ g^{\nu\mu'} & g^{\nu\nu'} & g^{\nu\alpha'} \\ g^{\alpha\mu'} & g^{\alpha\nu'} & g^{\alpha\alpha'} \end{vmatrix}, \quad (21)$$

the $\epsilon^{\mu\nu\alpha\beta} \epsilon^{\mu'\nu'\alpha'\beta'} k_\mu q_\alpha Q_{\mu'} q_{\alpha'} \epsilon_\nu \epsilon_{V\nu'}$ term of Eq. (20) is reduced to

$$\begin{aligned}
&\epsilon^{\mu\nu\alpha\beta} \epsilon^{\mu'\nu'\alpha'\beta'} k_\mu q_\alpha Q_{\mu'} q_{\alpha'} \epsilon_\nu \epsilon_{V\nu'} = -\epsilon_{V\mu} \epsilon_\nu \\
&\times \{ k \cdot Q q^2 g^{\mu\nu} + q \cdot Q k^\mu q^\nu + q \cdot k q^\mu Q^\nu \\
&- q \cdot k q \cdot Q g^{\mu\nu} - q^2 k^\mu Q^\nu - k \cdot Q q^\mu q^\nu \}. \quad (22)
\end{aligned}$$

In order to separate the divergent part in a convenient way, we write the bracket $\{\dots\}$ of Eq. (22), by adding and subtracting $q^2(k \cdot Q g^{\mu\nu} - k^\mu Q^\nu)/2$, in the following way:

$$\begin{aligned}
\{\dots\} &\equiv [k \cdot Q q^2 g^{\mu\nu} + q \cdot Q k^\mu q^\nu + q \cdot k q^\mu Q^\nu \\
&- q \cdot k q \cdot Q g^{\mu\nu} - q^2 k^\mu Q^\nu - k \cdot Q q^\mu q^\nu \\
&- \frac{1}{2} k \cdot Q q^2 g^{\mu\nu} + \frac{1}{2} q^2 k^\mu Q^\nu] \\
&+ \frac{1}{2} q^2 (k \cdot Q g^{\mu\nu} - k^\mu Q^\nu). \quad (23)
\end{aligned}$$

Now the square bracket $[\dots]$ term in Eq. (23) leads to a finite contribution after performing the Feynman parametrization since the divergent contributions coming from the q' terms of Eq. (13) cancel algebraically.

The remaining part coming from the last $q^2(k \cdot Q g^{\mu\nu} - k^\mu Q^\nu)/2$ term of Eq. (23) leads to a logarithmically divergent contribution which can be written in terms of the known two-meson loop function, $G(s, m_1, m_2)$, already used in the meson-meson unitarized scattering amplitude. Explicit expressions for $G(s, m_1, m_2)$ can be found, *e.g.*, in refs. [38,39]. Indeed, we can do the following transformation when considering the propagators present in Eq. (20):

$$\begin{aligned}
&\frac{1}{2} q^2 (k \cdot Q g^{\mu\nu} - k^\mu Q^\nu) \frac{1}{q^2 - M_2^2} \\
&\times \frac{1}{(q+k)^2 - m_1^2} \frac{1}{(Q-q)^2 - m_2^2} = \\
&\frac{1}{2} (k \cdot Q g^{\mu\nu} - k^\mu Q^\nu) \left(\frac{q^2 - M_2^2}{q^2 - M_2^2} + \frac{M_2^2}{q^2 - M_2^2} \right) \\
&\times \frac{1}{(q+k)^2 - m_1^2} \frac{1}{(Q-q)^2 - m_2^2}, \quad (24)
\end{aligned}$$

The term $\frac{M_2^2}{q^2 - M_2^2}$ in the big parenthesis leads to a convergent part while the $\frac{q^2 - M_2^2}{q^2 - M_2^2}$ term is proportional to the two meson loop function, $G((Q+k)^2)$, which can be properly regularized either with a cutoff [7] or with dimensional regularization [12,13]. The procedure followed here to write the divergent part in terms of the meson-meson loop function is similar to what was done in ref. [40] in a different context.

Therefore, gathering the convergent parts and keeping only the contributions to the d -term of Eq. (3), we get the following convergent d -coefficient:

$$\begin{aligned}
d_b^{\text{con}} &= -ABC g_{SP_1P_2} \frac{N_B N_C G'^2 F_V}{2M_1} e\lambda_{V_1} \frac{1}{32\pi^2} \\
&\times \int_0^1 dx \int_0^x dy \frac{1}{s' + i\epsilon} (Q^2(1-x)^2 - M_2^2) \quad (25)
\end{aligned}$$

where now $s' = Q^2x(1-x) + 2Q \cdot k(1-x)y + (m_2^2 - M_2^2)x + (M_2^2 - m_1^2)y - m_2^2$.
 while the contribution to the d -term from the divergent part is

$$d_b^{\text{div}} = -ABC g_{SP_1P_2} \frac{N_B N_C G'^2 F_V}{4M_1} e\lambda_{V_1} G(P^2, m_1, m_2). \quad (26)$$

The total amplitude for the radiative decay process is then obtained from Eq. (5) where $d = d_a + d_b^{\text{con}} + d_b^{\text{div}}$ from Eqs. (14), (25) and (26).

The radiative decay width of the scalar resonances into a vector meson and a photon is then readily obtained, taking the narrow resonance limit in a first step, by

$$\Gamma(M_S, M_V) = \frac{|\mathbf{k}|}{8\pi M_S^2} \Sigma |T|^2 = \frac{M_S^3}{32\pi} \left(1 - \frac{M_V^2}{M_S^2}\right)^3 |d|^2, \quad (27)$$

where M_S stands for the mass of the scalar meson.

In order to take into account the finite width of the scalar resonance and the final vector meson we fold the previous expression with their corresponding mass distributions:

$$\begin{aligned} \Gamma_{S \rightarrow V\gamma} &= \frac{1}{\mathcal{N}\pi^2} \int_{(M_S-2\Gamma_S)^2}^{(M_S+2\Gamma_S)^2} ds_S \int_{(M_V-2\Gamma_V)^2}^{(M_V+2\Gamma_V)^2} ds_V \\ &\times \text{Im} \left\{ \frac{1}{s_S - M_S^2 + iM_S\Gamma_S} \right\} \\ &\times \text{Im} \left\{ \frac{1}{s_V - M_V^2 + iM_V\Gamma_V} \right\} \\ &\times \Gamma(\sqrt{s_S}, \sqrt{s_V}) \Theta(\sqrt{s_S} - \sqrt{s_S^{\text{th}}}) \Theta(\sqrt{s_V} - \sqrt{s_V^{\text{th}}}), \end{aligned} \quad (28)$$

where Θ is the step function, $s_{S(V)}^{\text{th}}$ is the threshold for the dominant $S(V)$ decay channel and \mathcal{N} is the normalization factor of the spectral distributions:

$$\begin{aligned} \mathcal{N} &= \frac{1}{\pi^2} \int_{(M_S-2\Gamma_S)^2}^{(M_S+2\Gamma_S)^2} ds_S \int_{(M_V-2\Gamma_V)^2}^{(M_V+2\Gamma_V)^2} ds_V \\ &\times \text{Im} \left\{ \frac{1}{s_S - M_S^2 + iM_S\Gamma_S} \right\} \text{Im} \left\{ \frac{1}{s_V - M_V^2 + iM_V\Gamma_V} \right\} \end{aligned} \quad (29)$$

Advancing some results, the effect of the folding with the vector-meson spectral function has little influence in the radiative decay widths. On the contrary, the convolution with the scalar meson mass distribution is crucial for the decays of the f_0 , as we will explain in the Results section.

3 Results

In table 3 we show the contributions of the type-a and -b loops to the radiative decay widths under considera-

tion¹. The numbers besides the labels $\pi\pi$, $K\bar{K}$ and $\pi\eta$ are the decay widths that we would obtain had we used only the loops-a or -b where the scalar meson vertex is attached to $\pi\pi$, $K\bar{K}$ and $\pi\eta$ respectively. The other number in columns 2 and 3 is the global loop-a or loop-b contribution. The theoretical errors quoted in our final results have been obtained by doing a Monte-Carlo sampling of the parameters of the model within their uncertainties as have appeared along the text. We have checked that the largest source of error in the final results for the f_0 decays is the uncertainty considered in the pseudoscalar decay constant f , while the largest one in the a_0 decays comes from the uncertainty in the g_{a_0PP} couplings.

For the $f_0 \rightarrow \rho^0\gamma$ the $\pi\pi$ type-a loops contribution, in spite of being only a 10% of the $K\bar{K}$ one, influences the global loop-a contribution by about 30% due to the interference with the dominant $K\bar{K}$ type-a loop.

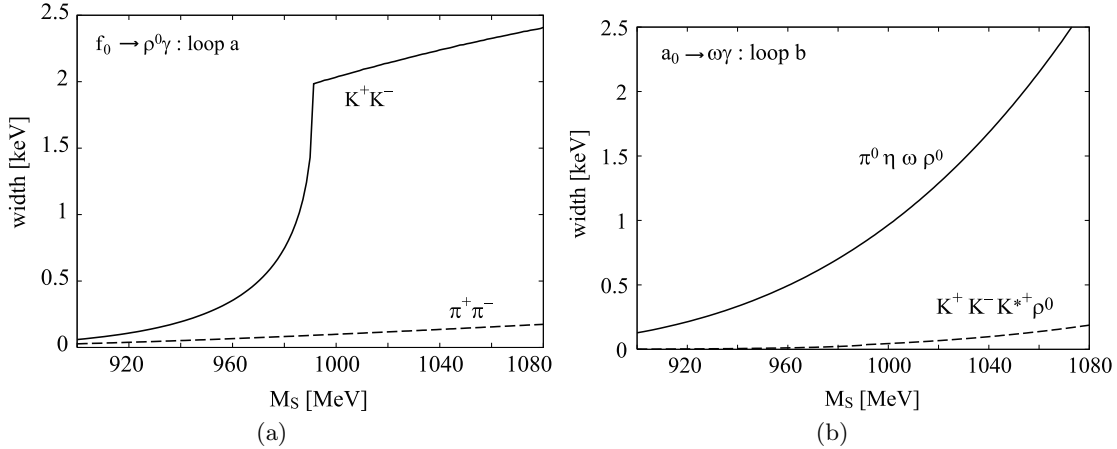
In table 3 we can see that the contribution of the type-b loops to the decay widths, evaluated for the first time in the present work, is quite important for most of the decays, particularly for the $f_0 \rightarrow \rho^0\gamma$, $a_0 \rightarrow \rho\gamma$ and $a_0 \rightarrow \omega\gamma$ decays. The $K\bar{K}$ loops in the type-b diagrams are small by themselves with respect to the $\pi\pi$ or $\pi\eta$ loops. However, they are important to give the global type-b contribution after the coherent interference with the $\pi\pi$ or $\pi\eta$ loops. For instance, had we only considered the type-a loops, the results would be the same for the $a_0 \rightarrow \rho\gamma$ and $a_0 \rightarrow \omega\gamma$ radiative decay widths. (The differences in table 3 are due to the different masses of ρ and ω). The type-b loops for these a_0 decays are dominated by the $\pi\eta$ loops. However, the $\pi\eta$ mechanisms of the type-b loops for the $a_0 \rightarrow \omega\gamma$ decay is one order of magnitude larger than that of the $a_0 \rightarrow \rho\gamma$. This is essentially due to the fact that the vector meson attached to the photon (V_1 in fig. 1b) is a ρ in the former case and an ω in the later one. This implies a factor three difference in the λ_{V_1} coefficient of the direct coupling of the vector meson to the photon (see Eq. (16)). This makes, after the interference with the other pieces, that the width of the $a_0 \rightarrow \omega\gamma$ decay is much larger than the $a_0 \rightarrow \rho\gamma$ decay width.

Since all these interference effects are so important, it is crucial to know the relative sign among the different couplings of the model. At this point the chiral unitary approach makes a decisive contribution since, as explained at the beginning of section 2, it provides the g_{SPP} couplings including their phase. Hence the right direction of the interferences among the different mechanisms is a genuine non-trivial prediction of UChPT.

On the other hand it is worth mentioning the importance of the convolution with the scalar mass distribution, Eq. (28). Had we not considered the folding of the decay width with the scalar meson spectral function we would have obtained radiative decay widths for the f_0 about 3 times smaller than in the case when the convolution is performed. Indeed, as already mentioned in refs. [1, 24] the loop functions for the type-a diagrams are strongly depen-

¹ By $a_0 \rightarrow \rho\gamma$ we denote both $a_0^0 \rightarrow \rho^0\gamma$ and $a_0^\pm \rightarrow \rho^\pm\gamma$ since the results are the same for both decays.

| | loop a | | loop b | | total |
|---------------------------------|--------------------------------------|------|--|------|---------------|
| $f_0 \rightarrow \rho^0 \gamma$ | $\pi\pi$: 0.44 $K\bar{K}$: 4.10 | 3.13 | $\pi\pi$: 1.82 $K\bar{K}$: 0.56 | 1.30 | 4.2 ± 1.1 |
| $f_0 \rightarrow \omega \gamma$ | $K\bar{K}$ | 4.31 | $\pi\pi$: 1.34 $K\bar{K}$: 0.013 | 1.49 | 4.3 ± 1.3 |
| $a_0 \rightarrow \rho \gamma$ | $K\bar{K}$ | 7.43 | $\pi\eta$: 0.68 $K\bar{K}$: 0.046 | 0.42 | 11 ± 4 |
| $a_0 \rightarrow \omega \gamma$ | $K\bar{K}$ | 7.85 | $\pi\eta$: 4.69 $K\bar{K}$: 0.79 | 9.23 | 31 ± 13 |

Table 3. Contribution of the different mechanisms to the radiative decay widths. All the units are in KeV.**Fig. 3.** Left panel: $f_0 \rightarrow \rho^0 \gamma$ decay width as a function of the scalar meson mass for the type-a loop. Solid line: $\pi^+ \pi^-$ loop; dashed line: $K^+ K^-$ loop. Right panel: $a_0 \rightarrow \omega \gamma$ decay width as a function of the scalar meson mass for the type-b loop. Solid line: $\pi^0 \eta \omega \rho^0$ loop; dashed line: $K^+ K^- K^{*+} \rho^0$ loop.

dent on the scalar meson mass. This is specially relevant for the f_0 decay channels.

In fig. 3 we show, as an example, the decay widths as a function of the scalar meson mass that one would obtain (without the convolution) for particular mechanisms for the type-a (fig. 3(a)) and type-b (fig. 3(b)) mechanisms. In fig. 3(a) one can see the strong dependence with the energy of the type-a kaon loops close to the $K\bar{K}$ threshold. This makes that small variations in the scalar meson mass change drastically the final radiative decay width. This is why it is very important to account properly for the scalar meson mass distribution by folding with the spectral function. For the type-a $\pi\pi$ loops and for the type-b, the dependence with the energy are smoother because, as seen in table 3, they are dominated by $\pi\pi$ or $\pi\eta$ $P_1 P_2$ mechanisms, which have the threshold far from the ~ 980 MeV region of interest. Therefore, the influence of the convolution with the scalar mass distribution is less relevant for the type-b loops.

At this point it is worth commenting about the relative size of the divergent and convergent part of the type-b loops. We have checked that by using in the evaluation of the decay widths only the convergent (Eq. 25) or divergent (Eq. 26) part, the contribution from the type-b loops would be from 3 to 10 times larger (depending on the channels) than those given in table 3. However, the sign

of d_b^{div} is opposite to that of d_b^{conv} and then a strong destructive interference results leading to the type-b contributions shown in table 3.

Finally, in table 4 we compare our result with other theoretical determinations. The model [1](I) is based on quark models, ref. [1](II) on kaon loops, ref. [23](I) and (II) on VMD from direct SVP contact term and ref. [24] on meson loops by using the resonance Lagrangians of [31].

We can see the wide dispersion among the different theoretical models. The previous calculations dealing with meson loops, refs. [1](II) and [24], do not include the type-b loops considered in the present work. The model of ref. [1](II) neglects the pion loops for the type-a mechanisms which, as shown above and despite being small by themselves, affects the final result of the radiative decay widths in a significant manner after the coherent addition to the dominant contributions. On the other hand, the model [1](II) relies on an estimation of the g_{SPP} that *should be viewed as qualitative* [sic] [1] and the model of [24] uses couplings from the resonance Lagrangian of [31] which we questioned before. On the contrary, the chiral unitary approach provides precise values for the couplings, including their phase, which have been successfully tested in many processes, and have uncertainties under control. In any case we should stress that all the results from the meson loops are of the same order of magnitude, and quite different from the quark and VMD models.

| | [1](I) | [1](II) | [23](I) | [23](II) | [24] | present work |
|---------------------------------|--------|---------|---------------|---------------|------|---------------|
| $f_0 \rightarrow \rho^0 \gamma$ | 125 | 3 | 19 ± 5 | 3.3 ± 2.0 | 9.6 | 4.2 ± 1.1 |
| $f_0 \rightarrow \omega \gamma$ | 14 | 3 | 126 ± 20 | 88 ± 17 | 15.0 | 4.3 ± 1.3 |
| $a_0 \rightarrow \rho \gamma$ | 14 | 3 | 3.0 ± 1.0 | 3.0 ± 1.0 | 9.1 | 11 ± 4 |
| $a_0 \rightarrow \omega \gamma$ | 125 | 3 | 641 ± 87 | 641 ± 87 | 8.7 | 31 ± 13 |

Table 4. Comparison of the radiative decay widths with other theoretical predictions. All the units are in KeV.

The large dispersion among the theoretical models stresses the extreme sensitivity of these radiative decays to the theoretical models and on the nature of these resonances. Hence, an experimental measurement would be very valuable to discern among theoretical models. The numerical values obtained here are within reach in present experimental facilities, in particular at COSY/Juelich where an experiment is already approved [26].

4 Summary

We have evaluated the radiative decays of the $a_0(980)$ and $f_0(980)$ scalar mesons into a vector meson and one photon from the point of view of the chiral unitary approach, where the $a_0(980)$ and $f_0(980)$ scalar mesons are dynamically generated by implementing unitarity in coupled channels in the pseudoscalar-pseudoscalar interaction. By evaluating the residues at the pole positions in unphysical Riemann sheets of the partial wave amplitudes, the couplings of the scalar mesons to the different PP channels can be obtained both in modulus and phase. Within this dynamical framework, the natural way to evaluate the radiative decay widths is to consider the decay of the scalar mesons into their constituent PP building blocks and then allow the photon to be emitted from the pseudoscalar legs of the allowed loops. We consider not just the mechanisms with only pseudoscalar mesons in the loops, but also those with a vector meson in the loop. By using arguments of gauge invariance we show that the contribution of the loops involving only pseudoscalar mesons, which are in most of the cases the dominant ones, are convergent. The loops containing a vector meson are logarithmically divergent, but this divergence can be recast into the two meson-loop function used in the scattering process, well under control, which leads to the dynamical generation of the scalar resonances.

We make predictions for all the allowed $f_0/a_0 \rightarrow V\gamma$ decay widths including also an error analysis from the uncertainties in the parameters of the model. We show that even if some of the mechanisms are small by themselves, like the pion loops for the $f_0 \rightarrow \rho^0 \gamma$ or the loops containing a vector meson in the loop, they affect strongly the final results due to non-trivial interferences with the dominant mechanisms. The sign of these interferences are well under control thanks to the knowledge of the phase of the couplings provided by the underlying unitary theory that generates dynamically the scalar resonances.

These radiative decays are very sensitive to details of the models, hence an experimental measure would be

highly valuable to discern among theoretical models. The COSY/WASA [26] scheduled experiment should be very useful in this respect.

Acknowledgments

We thank financial support from MEC (Spain) grants No. FPA2004-03470, FIS2006-03438, FPA2007-62777, Fundación Séneca grant No. 02975/PI/05, and the Japan(JSPS)-Spain collaboration agreement. One of the author (H.N.) is the Research Fellow of the Japan Society for the Promotion of Science (JSPS) and supported by the Grant for Scientific Research from JSPS (No. 18-8661). This research is part of the EU Integrated Infrastructure Initiative Hadron Physics Project under contract number RII3-CT-2004-506078.

References

1. Yu. Kalashnikova, A. E. Kudryavtsev, A. V. Nefediev, J. Haidenbauer and C. Hanhart, Phys. Rev. C **73** (2006) 045203.
2. Z. G. Wang, Phys. Rev. D **75** (2007) 034013.
3. S. Godfrey, Phys. Lett. B **568**, 254 (2003); P. Colangelo and F. De Fazio, Phys. Lett. B **570**, 180 (2003); W. A. Bardeen, E. J. Eichten and C. T. Hill, Phys. Rev. D **68**, 054024 (2003); Fayyazuddin and Riazuddin, Phys. Rev. D **69**, 114008 (2004); S. Ishida, M. Ishida, T. Komada, T. Maeda, M. Oda, K. Yamada and I. Yamauchi, AIP Conf. Proc. **717**, 716 (2004); Y. I. Azimov and K. Goeke, Eur. Phys. J. A **21**, 501 (2004); P. Colangelo, F. De Fazio and A. Ozpineci, Phys. Rev. D **72**, 074004 (2005); F. E. Close and E. S. Swanson, Phys. Rev. D **72**, 094004 (2005); X. Liu, Y. M. Yu, S. M. Zhao and X. Q. Li, Eur. Phys. J. C **47**, 445 (2006); Z. G. Wang, J. Phys. G **34**, 753 (2007); D. Gamermann, L. R. Dai and E. Oset, Phys. Rev. C **76** (2007) 055205; M. F. M. Lutz and M. Soyeur, arXiv:0710.1545 [hep-ph].
4. E. van Beveren, T. A. Rijken, K. Metzger, C. Dullemond, G. Rupp and J. E. Ribeiro, Z. Phys. C **30** (1986) 615.
5. D. Black, A. H. Fariborz, F. Sannino and J. Schechter, Phys. Rev. D **59** (1999) 074026.
6. N. A. Tornqvist, Z. Phys. C **68** (1995) 647.
7. J. A. Oller and E. Oset, Nucl. Phys. A **620**, 438 (1997) [Erratum-ibid. A **652**, 407 (1999)].
8. J. Gasser and H. Leutwyler, Nucl. Phys. B **250** (1985) 465.
9. N. Kaiser, Eur. Phys. J. A **3** (1998) 307.
10. V. E. Markushin, Eur. Phys. J. A **8** (2000) 389.
11. J. Nieves and E. Ruiz Arriola, Nucl. Phys. A **679** (2000) 57.
12. J. A. Oller and E. Oset, Phys. Rev. D **60** (1999) 074023.

13. J. A. Oller, E. Oset and J. R. Pelaez, Phys. Rev. D **59** (1999) 074001 [Erratum-ibid. D **60** (1999) ER-RAT,D75,099903.2007) 099906].
14. J. R. Pelaez, Phys. Rev. Lett. **92** (2004) 102001.
15. E. Marco, S. Hirenzaki, E. Oset and H. Toki, Phys. Lett. B **470** (1999) 20.
16. J. E. Palomar, L. Roca, E. Oset and M. J. Vicente Vacas, Nucl. Phys. A **729** (2003) 743.
17. J. A. Oller and E. Oset, Nucl. Phys. A **629** (1998) 739.
18. J. A. Oller and L. Roca, Phys. Lett. B **651** (2007) 139.
19. C. b. Li, E. Oset and M. J. Vicente Vacas, Phys. Rev. C **69** (2004) 015201.
20. U. G. Meissner and J. A. Oller, Nucl. Phys. A **679** (2001) 671.
21. L. Roca, J. E. Palomar, E. Oset and H. C. Chiang, Nucl. Phys. A **744** (2004) 127.
22. J. A. Oller, E. Oset and A. Ramos, Prog. Part. Nucl. Phys. **45** (2000) 157.
23. D. Black, M. Harada and J. Schechter, Phys. Rev. Lett. **88** (2002) 181603.
24. S. Ivashyn and A. Y. Korchin, arXiv:0707.2700 [hep-ph].
25. J. E. Palomar, S. Hirenzaki and E. Oset, Nucl. Phys. A **707** (2002) 161.
26. P. Fedorets and M-Büscher,
http://www.fz-juelich.de/ikp/publications/List_of_all_COSY-Proposals.shtml
27. J. A. Oller, Nucl. Phys. A **727** (2003) 353.
28. F. E. Close, N. Isgur and S. Kumano, Nucl. Phys. B **389** (1993) 513.
29. L. Roca, A. Hosaka and E. Oset, Phys. Lett. B **658** (2007) 17.
30. H. Nagahiro, L. Roca and E. Oset, Phys. Rev. D in print.
31. G. Ecker, J. Gasser, A. Pich and E. de Rafael, Nucl. Phys. B **321** (1989) 311.
32. F. Mandl and G. Shaw, Quantum Field Theory, John Wiley and Sons, 1984
33. Yu. S. Kalashnikova, A. E. Kudryavtsev, A. V. Nefediev, C. Hanhart and J. Haidenbauer, Eur. Phys. J. A **24** (2005) 437.
34. S. Weinberg, Phys. Rev. **130** (1963) 776.
35. A. Bramon, A. Grau and G. Pancheri, Phys. Lett. B **283** (1992) 416.
36. E. Oset, J. R. Pelaez and L. Roca, Phys. Rev. D **67** (2003) 073013.
37. W.-M. Yao et al. (Particle Data Group), J. Phys. G **33**, 1 (2006) and 2007 partial update for the 2008 edition
38. J. A. Oller and U. G. Meissner, Phys. Lett. B **500** (2001) 263.
39. L. Roca, E. Oset and J. Singh, Phys. Rev. D **72** (2005) 014002.
40. M. Napsuciale, E. Oset, K. Sasaki and C. A. Vaquera-Araujo, Phys. Rev. D **76** (2007) 074012.

A Numerical coefficients

| decay | $P_1 P_2$ | A | C |
|-----------------------------------|---------------|---------------|---------------|
| $f_0 \rightarrow \rho_0 \gamma$ | $\pi^+ \pi^-$ | $-\sqrt{2/3}$ | $-\sqrt{2}$ |
| | $\pi^- \pi^+$ | $-\sqrt{2/3}$ | $\sqrt{2}$ |
| | $K^+ K^-$ | $-1/\sqrt{2}$ | $-1/\sqrt{2}$ |
| | $K^- K^+$ | $-1/\sqrt{2}$ | $1/\sqrt{2}$ |
| $f_0 \rightarrow \omega \gamma$ | $K^+ K^-$ | $-1/\sqrt{2}$ | $-1/\sqrt{2}$ |
| | $K^- K^+$ | $-1/\sqrt{2}$ | $1/\sqrt{2}$ |
| $a_0^0 \rightarrow \rho_0 \gamma$ | $K^+ K^-$ | $-1/\sqrt{2}$ | $-1/\sqrt{2}$ |
| | $K^- K^+$ | $-1/\sqrt{2}$ | $1/\sqrt{2}$ |
| $a_0^0 \rightarrow \omega \gamma$ | $K^+ K^-$ | $-1/\sqrt{2}$ | $-1/\sqrt{2}$ |
| | $K^- K^+$ | $-1/\sqrt{2}$ | $1/\sqrt{2}$ |
| $a_0^+ \rightarrow \rho^+ \gamma$ | $K^+ K^0$ | -1 | -1 |

Table 5. Coefficients of Eq. (14) for type-a diagrams

| decay | $P_1 P_2 V_2 V_1$ | A | B | C |
|---------------------------------|-----------------------------|---------------|---------------|---------------|
| $f_0 \rightarrow \rho_0 \gamma$ | $\pi^0 \pi^0 \omega \rho^0$ | $-\sqrt{2/3}$ | $\sqrt{2}$ | $\sqrt{2}$ |
| | $K^+ K^- K^{*+} \rho^0$ | $-1/\sqrt{2}$ | $1/\sqrt{2}$ | $1/\sqrt{2}$ |
| | ω | | $1/\sqrt{2}$ | |
| | ϕ | | 1 | |
| | $K^- K^+ K^{*-} \rho^0$ | $-1/\sqrt{2}$ | $1/\sqrt{2}$ | $1/\sqrt{2}$ |
| | ω | | $1/\sqrt{2}$ | |
| | ϕ | | 1 | |
| | $K^0 K^0 K^{*0} \rho^0$ | $-1/\sqrt{2}$ | $-1/\sqrt{2}$ | $-1/\sqrt{2}$ |
| | ω | | $1/\sqrt{2}$ | |
| | ϕ | | 1 | |
| | $K^0 K^0 K^{*0} \rho^0$ | $-1/\sqrt{2}$ | $-1/\sqrt{2}$ | $-1/\sqrt{2}$ |
| | ω | | $1/\sqrt{2}$ | |
| ϕ | | 1 | | |
| $f_0 \rightarrow \omega \gamma$ | $\pi^+ \pi^- \rho^+ \omega$ | $-\sqrt{2/3}$ | $\sqrt{2}$ | $\sqrt{2}$ |
| | $\pi^- \pi^+ \rho^- \omega$ | $-\sqrt{2/3}$ | $\sqrt{2}$ | $\sqrt{2}$ |
| | $\pi^0 \pi^0 \rho^0 \omega$ | $-\sqrt{2/3}$ | $\sqrt{2}$ | $\sqrt{2}$ |
| | $K^+ K^- K^{*+} \rho^0$ | $-1/\sqrt{2}$ | $1/\sqrt{2}$ | $1/\sqrt{2}$ |
| | ω | | $1/\sqrt{2}$ | |
| | ϕ | | 1 | |
| | $K^- K^+ K^{*-} \rho^0$ | $-1/\sqrt{2}$ | $1/\sqrt{2}$ | $1/\sqrt{2}$ |
| | ω | | $1/\sqrt{2}$ | |
| | ϕ | | 1 | |
| | $K^0 K^0 K^{*0} \rho^0$ | $-1/\sqrt{2}$ | $-1/\sqrt{2}$ | $1/\sqrt{2}$ |
| | ω | | $1/\sqrt{2}$ | |
| | ϕ | | 1 | |
| $K^0 K^0 K^{*0} \rho^0$ | $-1/\sqrt{2}$ | $-1/\sqrt{2}$ | $1/\sqrt{2}$ | |
| ω | | $1/\sqrt{2}$ | | |
| ϕ | | 1 | | |

Table 6. Coefficients A, B and C of Eq. (19) for the different allowed type-b diagrams. The continuation is in table 7...

| decay | $P_1 P_2 V_2 V_1$ | A | B | C | |
|-----------------------------------|-----------------------------------|-------------------------|---------------|---------------|--------------|
| $a_0^0 \rightarrow \rho_0 \gamma$ | $K^+ K^- K^{*+} \rho^0$ | $-1/\sqrt{2}$ | $1/\sqrt{2}$ | $1/\sqrt{2}$ | |
| | ω | | $1/\sqrt{2}$ | | |
| | ϕ | | 1 | | |
| | $K^- K^+ K^{*-} \rho^0$ | $-1/\sqrt{2}$ | $1/\sqrt{2}$ | $1/\sqrt{2}$ | |
| | ω | | $1/\sqrt{2}$ | | |
| | ϕ | | 1 | | |
| | $K^0 K^0 K^{*0} \rho^0$ | $1/\sqrt{2}$ | $-1/\sqrt{2}$ | $-1/\sqrt{2}$ | |
| | ω | | $1/\sqrt{2}$ | | |
| | ϕ | | 1 | | |
| | $K^0 K^0 K^{*0} \rho^0$ | $1/\sqrt{2}$ | $-1/\sqrt{2}$ | $-1/\sqrt{2}$ | |
| | ω | | $1/\sqrt{2}$ | | |
| | ϕ | | 1 | | |
| $a_0^0 \rightarrow \omega \gamma$ | $\pi^0 \eta \rho^0 \omega$ | 1 | $\sqrt{2}$ | $\sqrt{2/3}$ | |
| | $\eta \pi^0 \omega \omega$ | 1 | $\sqrt{2/3}$ | $\sqrt{2}$ | |
| | $a_0^+ \rightarrow \rho^+ \gamma$ | $K^+ K^- K^{*+} \rho^0$ | $-1/\sqrt{2}$ | $1/\sqrt{2}$ | $1/\sqrt{2}$ |
| | | ω | | $1/\sqrt{2}$ | |
| | | ϕ | | 1 | |
| | $a_0^+ \rightarrow \rho^+ \gamma$ | $K^- K^+ K^{*-} \rho^0$ | $-1/\sqrt{2}$ | $1/\sqrt{2}$ | $1/\sqrt{2}$ |
| ω | | | $1/\sqrt{2}$ | | |
| ϕ | | | 1 | | |
| $a_0^+ \rightarrow \rho^+ \gamma$ | $K^0 K^0 K^{*0} \rho^0$ | $1/\sqrt{2}$ | $-1/\sqrt{2}$ | $1/\sqrt{2}$ | |
| | ω | | $1/\sqrt{2}$ | | |
| | ϕ | | 1 | | |
| $a_0^+ \rightarrow \rho^+ \gamma$ | $K^0 K^0 K^{*0} \rho^0$ | $1/\sqrt{2}$ | $-1/\sqrt{2}$ | $1/\sqrt{2}$ | |
| | ω | | $1/\sqrt{2}$ | | |
| | ϕ | | 1 | | |
| $a_0^+ \rightarrow \rho^+ \gamma$ | $\pi^0 \eta \omega \rho^0$ | 1 | $\sqrt{2}$ | $\sqrt{2/3}$ | |
| | $\eta \pi^0 \rho^0 \rho^0$ | 1 | $\sqrt{2/3}$ | $\sqrt{2}$ | |
| | $a_0^+ \rightarrow \rho^+ \gamma$ | $K^+ K^0 K^{*+} \rho^0$ | -1 | $1/\sqrt{2}$ | 1 |
| ω | | | $1/\sqrt{2}$ | | |
| ϕ | | | 1 | | |
| $a_0^+ \rightarrow \rho^+ \gamma$ | $K^0 K^+ K^{*0} \rho^0$ | -1 | $-1/\sqrt{2}$ | 1 | |
| | ω | | $1/\sqrt{2}$ | | |
| | ϕ | | 1 | | |
| $a_0^+ \rightarrow \rho^+ \gamma$ | $\pi^+ \eta \rho^+ \omega$ | 1 | $\sqrt{2}$ | $\sqrt{2/3}$ | |
| | $\eta \pi^+ \omega \omega$ | 1 | $\sqrt{2/3}$ | $\sqrt{2}$ | |

Table 7. ... continuation of table 6.